American Mineralogist, Volume 80, pages 1302–1306, 1995

Techniques for determining pressure in the hydrothermal diamond-anvil cell: Behavior and identification of ice polymorphs (I, III, V, VI)

H. T. Haselton, Jr., I-Ming Chou
U.S. Geological Survey, 959 National Center, Reston, Virginia 22092, U.S.A.
A. H. Shen,* W. A. Bassett
Department of Geological Sciences, Cornell University, Ithaca, New York 14853, U.S.A.

Abstract

For H_2O densities > 1.0 g/cm³, a determination of the ice melting temperature provides the density information required to calculate the P-T path that the sample in a hydrothermal diamond-anvil cell follows when the sample is heated isochorically. The principal difficulty is the identification of the polymorph because of metastable behavior of ices in the H_2O system. Usually, an accurate identification of the liquidus ice phase can be made without analytical instrumentation and requires only careful observations.

Introduction

The hydrothermal diamond-anvil cell (HDAC) is an advantageous experimental tool because the sample can be seen by light microscopy, and many types of analytical techniques can be applied while the sample is at high pressures and temperatures; however, the difficulty of determining the pressure precisely and accurately is a critical limitation that has prevented its widespread use in hydrothermal studies. In recent work, Shen et al. (1993) demonstrated a technique for determining pressure that may have wide applicability. They showed that during heating or cooling, the sample volume in the HDAC can be held constant within ±1%. Therefore, if the density of the fluid sample is known at one P-T condition and an accurate equation of state (EOS) is available, the isochoric P-T path traversed by the sample during heating or cooling can be calculated. In their test application of this idea, Shen et al. (1993) placed a doubly polished quartz chip in the HDAC with H_2O as the pressure medium. At low temperature, the H_2O density was calculated from the liquid-vapor homogenization temperature (T_h). On the basis of this density, P-T paths were calculated from various equations of state for H_2O. At a higher temperature, the α-β quartz transition, which was observed as an abrupt shift in the fringes of a laser interference pattern, provided a second P-T calibration point. The intersection of a calculated, isochoric P-T path with the α-β quartz transition curve yields a temperature that can be compared with the observed transition temperature. They concluded that, of the equations considered, the EOS of H_2O formulated by Haar et al. (1984) gave the best prediction of the α-β quartz transition temperature from the observed T_h. Although T_h continued to decrease slightly as the temperature was cycled between the liquid-vapor homogenization and α-β quartz transition temperatures because of gasket relaxation (Shen, unpublished data), the sample volume followed an isochore to a very good approximation after the first heating.

In experiments employing H_2O densities > 1.0 g/cm³, the solid-liquid boundaries of H_2O provide an excellent means of determining the density of an isochore. Wagner et al. (1994) critically evaluated available experimental measurements for the ice-liquid boundaries, corrected these data for changes in the pressure and temperature scales, and presented equations that represent the ice-liquid boundaries to pressures of about 200 kbar, the upper limit of the experimental measurements.

With regard to calculating H_2O densities along the ice boundaries, the equations of Haar et al. (1984) and Saul and Wagner (1989) yield small, systematic deviations from the pressure-corrected data of Bridgman (1912). Of greater concern is the divergence of isochores calculated from these equations at higher temperatures (Fig. 1). For example, in the postulated P-T region for the genesis of blueschist-facies metamorphic rocks, ultrahigh pressures and moderate temperatures (e.g., Sharp et al., 1993; Zhang and Liou, 1994), the divergence is considerable. A possible explanation was offered by Saul and Wagner (1989) who noted that the EOS of Haar et al. (1984) exhibits anomalous behavior, a crossing of calculated isotherms, at very high pressures and low temperatures. The results of a study based on synthetic fluid inclusions in corundum by Brodholt and Wood (1994) also suggest that the EOS of Saul and Wagner (1989) is more accurate than the equation of Haar et al. (1984). On the other hand, the experiments of Shen et al. (1993) at temperatures and pressures up to 850 °C and 11 kbar indicate that the Haar et al. (1984) EOS may be more accurate. At present, despite the technical improvements of the Saul and Wagner (1989) equation, it is not an unequivocal choice for per-

* Present address: Bayerisches Geoinstitut, Universität Bayreuth, D-95440 Bayreuth, Germany.

0003–004X/95/1112–1302$02.00

forming geologic calculations at all temperatures and pressures. If neither the Haar et al. (1984) nor the Saul and Wagner (1989) EOS appears suitable for a particular application, one of the many equations (e.g., Halbach and Chatterjee, 1982; Duan et al., 1992; Brodholt and Wood, 1993) that has been formulated for use only at high *P-T* conditions may be substituted for the high *P-T* part of the isochore calculation.

The problem of correctly identifying ice polymorphs in the HDAC is complicated by the metastability of some of the phases and the apparent shifting of some of the phase boundaries as a result. The purpose of this study is to provide a guide to the criteria that can be applied with confidence to the identification of the pertinent ice phases and melting curves. When these phases and curves are properly identified, they provide an accurate and reliable means of producing the desired pressure-temperature conditions for the study of hydrothermal systems.

Experimental details

The HDAC used in our work was designed by Bassett et al. (1993) for use in hydrothermal studies. Briefly, a type-K thermocouple (0.076 mm diameter wire) was cemented to each diamond anvil adjacent to the sample space. Thermocouples were calibrated in situ at the triple point of H_2O (0.01 °C) and the melting point of $NaNO_3$ (306.8 °C). The ice I–ice III–liquid triple point at −21.985 °C (Wagner et al., 1994) is a convenient secondary calibration point. The temperature of the bottom diamond more accurately reflects the melting-point temperature in the HDAC because the crystal is usually in contact only with the bottom diamond. However, the condensation behavior of large vapor bubbles that touch both anvil faces provides a sensitive means of detecting temperature gradients between anvils. We consider reported temperatures to be accurate to ±0.2 °C.

The temperature of the sample was controlled by either of two methods. For temperatures below ambient, the sample was cooled by directing a stream of cold nitrogen gas at the diamond anvils. The flow rate and the approximate temperature of the gas stream were controlled by a system that allows mixing of cold nitrogen gas and liquid. With this system, the sample can be rapidly cooled to near liquid nitrogen temperature, and, in the range of about −40 to 20 °C, the temperature can be controlled with a variation of <0.1 °C. At temperatures above ambient, the sample is heated by means of Mo resistance heaters wound on the tungsten carbide anvil seats. Thermocouples are interfaced to a PC-AT compatible computer, and temperatures are overlaid on the video record of the experiment (Haselton and Chou, 1994). The gasket was 125 μm thick rhenium foil with a 500 μm diameter hole that was drilled with a Q-switched Nd:YAG laser.

In most experiments, a small chip of $BaTiO_3$ was loaded into the cell with deionized, distilled water. Several *P-T* traverses were made between the ice nucleation temperature and the tetragonal to cubic transition temperature of $BaTiO_3$ before tightening the cell again. In experiments in which a crystal of $BaTiO_3$ was present, the tetragonal to cubic transitional temperature was also used to calculate a pressure and density (Chou et al., 1993). We saw no evidence of significant $BaTiO_3$ dissolution, such as pitting or precipitation of cystallites; therefore, we assume that the presence of $BaTiO_3$ does not affect H_2O phase relations. This second density determination provided a check on our identification of the liquidus ice phase. Our interpretation of these freezing experiments is based on visual observation; we collected no spectroscopic data. Typically, ice nucleated at 15–40 °C below the melting point, and, on a specific isochore, the amount of supercooling required for nucleation of ice usually was reproducible to within a few degrees.

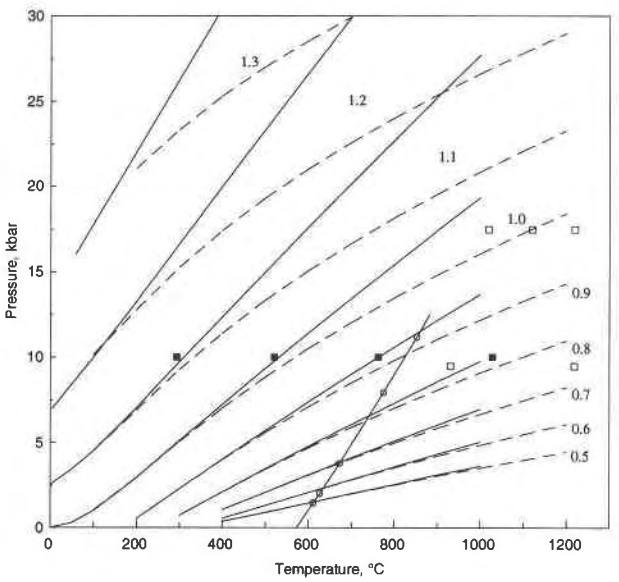

Fig. 1. Selected isochores for high-density liquid H_2O, 0.5–1.3 g/cm³, calculated from the Haar et al. (1984, dashed curves) and Saul and Wagner (1989, solid curves) equations of state. Neither equation of state was extrapolated beyond the recommended *P-T* range. The temperatures corresponding to selected densities in the range 0.8–1.1 g/cm³ at 10 kbar from Burnham et al. (1969) are shown by solid squares. Open squares are the *P-T* conditions of the lower temperature experiments of Brodholt and Wood (1994), and open circles are the *P-T* conditions of observations of the α-β quartz transition by Shen et al. (1993) determined from the equation of Mirwald and Massonne (1980).

The precise beginning of ice melting in the HDAC can be quite difficult to detect, especially when the density is not close to a triple point. Probably because the temperature gradient between anvils is larger than that across the sample space, the initial liquid occurs as a thin film on a diamond face. Until ice begins to retreat from the inside rim of the gasket, the liquid phase does not have a clearly discernible boundary. Although the initial liquid cannot be seen, a distinct coarsening of grain texture is a reliable signal of its presence.

Certainly for liquid-absent assemblages, some nonhydrostatic stress is present in these experiments, but we

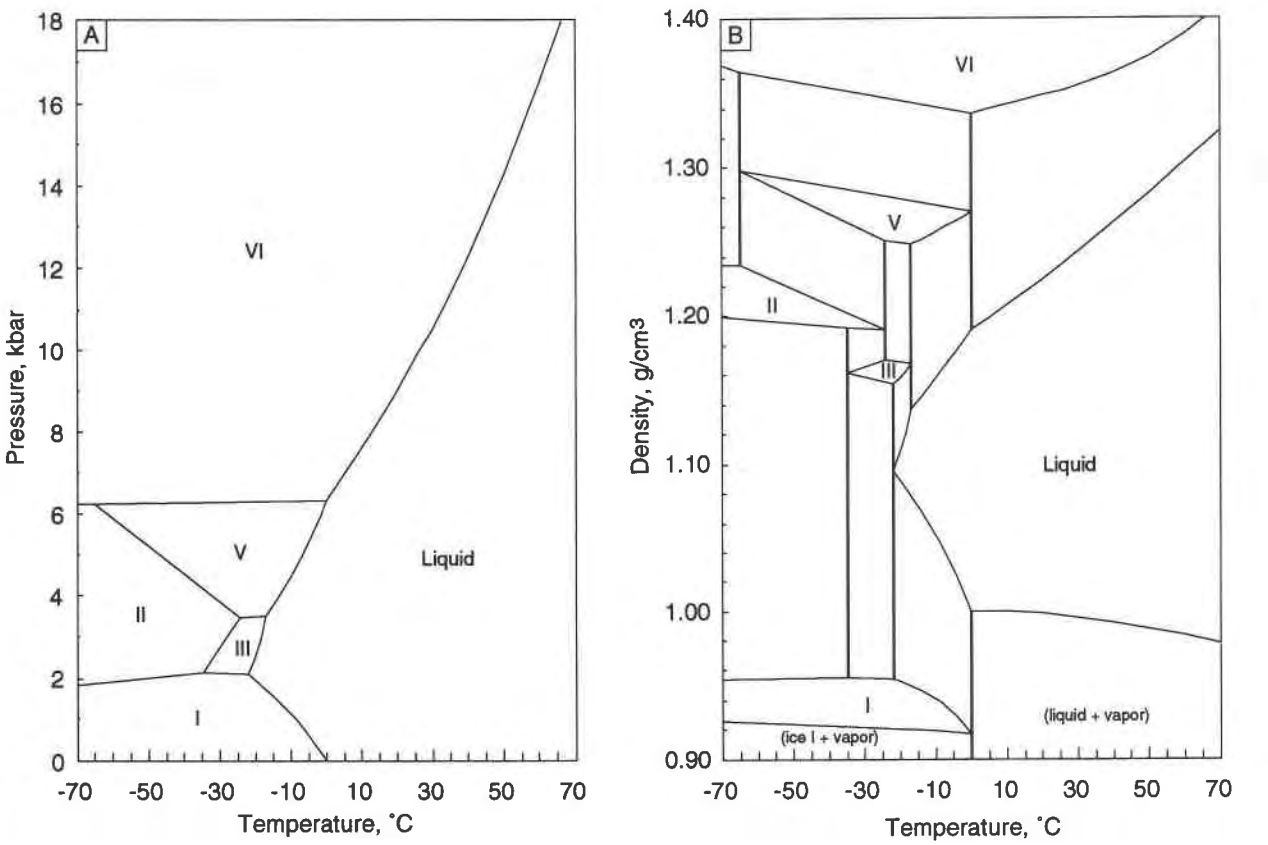

Fig. 2. (**A**) Pressure-temperature and (**B**) density-temperature phase diagrams for H_2O. Ice IV does not appear because it is not a stable phase.

cannot assess its significance. We did not make long-duration observations of liquid-absent assemblages to observe deformation or recrystallization that could be attributed to nonhydrostatic stress.

Results and discussion

Because the HDAC is essentially a constant-volume device, a density-temperature plot (Fig. 2B) of H_2O phase relations is a more appropriate representation of phase relations than a pressure-temperature diagram (Fig. 2A). In addition to giving information about proportions of phases at a specific density, a density-T plot is more useful than a P-T plot in unraveling metastable behavior. In drawing the density-T diagram, liquid densities were calculated by means of Wagner et al. (1994) and Saul and Wagner (1989). The densities of corresponding ice phases are given by Bridgman (1912). Volumes as a function of temperature are also given by Bridgman (1912) for most subsolidus reactions, but because the PVT properties are not known for ice II, ice III, and ice V, the extents of one-phase fields are less certain at lower temperatures. The most uncertain aspect of the density-T diagram is the position of the ice II–ice V–ice VI three-phase line; although, the density changes on the ice II–ice V and ice V–ice VI boundaries are well known. Of course, the diagrams in Figure 2 represent stable equilibrium phase relations, but ice-liquid metastable relations can be approximated by smooth extensions of appropriate boundaries.

Typical growth habits of ice I, ice III, ice V, and ice VI on the liquidus are shown in Figure 3. Ice I (Fig. 3A) grows as elongated blades that have low negative optical relief. Ice III (Fig. 3B) grows as approximately equidimensional thin plates that have low positive optical relief. The growth habits of ice I and ice III are sufficiently distinct as to be diagnostic. The optical relief of ice V (Fig. 3C) and ice VI (Fig. 3D) is significantly greater than that of ice I and ice III. Ice V crystals tend to be tabular, whereas ice VI crystals tend to be more equant and sometimes form pseudo-octahedra. The birefringence of all these polymorphs is low. In some instances, we were not confident of our ability to distinguish ice polymorphs in a density range near the ice V–ice VI–liquid triple point.

Metastable behavior of ice polymorphs has been observed in many studies, and the observed phenomena are dependent on the type of apparatus (e.g., Bridgman, 1912; Evans, 1967). We encountered metastable phase relations in almost all freezing experiments except at liquidus pressures exceeding about 10 kbar. First, with pure water in the HDAC, we observed ice II infrequently. Of the ice

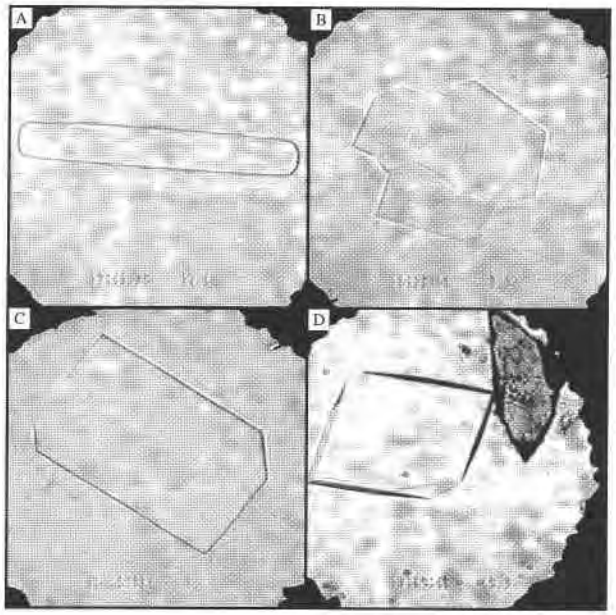

Fig. 3. Examples of the morphology of ices grown on the liquidus. The contrast of the video images was increased, and some mottling resulting from the outside surface of the top diamond was edited. (**A**) Ice I at −16.0 °C, (**B**) ice III at −20.8 °C, (**C**) ice V at −5.9 °C, and (**D**) ice VI at 50.0 °C with a crystal of barium titanate. Field of view is about 0.5 mm. The barely discernible temperatures on the images were not corrected.

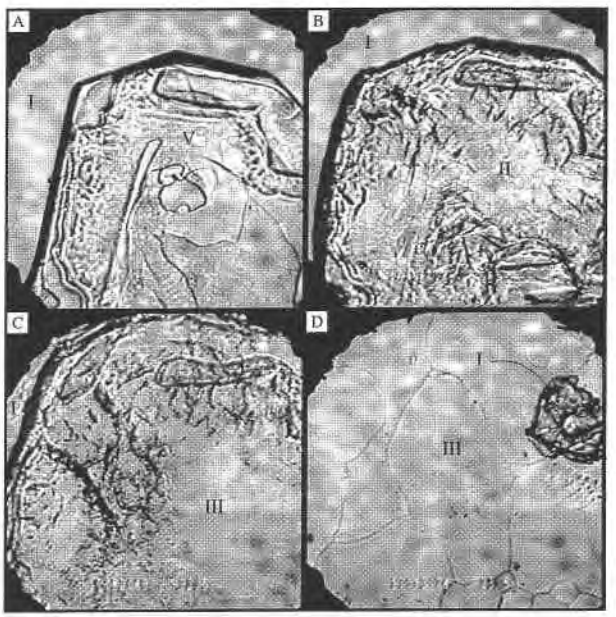

Fig. 4. Sequence of images for a freezing experiment at a bulk density of 1.13 g/cm³. (**A**) Ice I and ice V at −48.5 °C, (**B**) ice I and ice II at −68.9 °C, (**C**) ice I and ice III at −31.1 °C, and (**D**) ice III, a remnant of ice I, and liquid at −22.1 °C. Field of view is about 0.5 mm. The barely discernible temperatures on the images were not corrected.

phases discussed here, only ice II has ordered protons that may reduce the probability of ice II nucleation. One result of the failure of ice II to nucleate is that, for a large density range, ice I and ice V often nucleate together. As the temperature increases, ice III also often fails to nucleate; hence, liquidus temperatures for ice I are observed below the minimum melting point of −21.985 °C (Wagner et al., 1994). A diagnostic feature of the coexistence of ice I and ice V is melting at about −27.5 °C, the metastable ice I–ice V–liquid triple point.

At liquidus pressures of about 2–4 kbar, ice III tends to replace ice V during warming subsequent to the nucleation of ice I and ice V, so that ice III is the liquidus phase. In some experiments, ice III was the liquidus phase at temperatures above the ice III–ice V–liquid triple point, for which the likely interpretation is that ice III nucleated initially with ice I instead of ice I with ice V or the stable assemblage ice I and ice II. At liquidus pressures above the ice V–ice VI–liquid triple point (6324 bar, 0.16 °C), ice VI is the liquidus phase, though ice VI sometimes occurs at lower pressures because of the failure of ice V to nucleate.

In Figure 4A–4D, we show a sequence of images from a melting-point determination at a bulk density of 1.13 g/cm³ that displays some typical metastable behavior. In this experiment, two ice phases nucleated: ice I at −49 °C and ice V at −51 °C. On warming, liquid appeared at about −27.6 °C, indicating the presence of the metastable assemblage ice I + ice V + liquid. The temperature was then decreased, and, at about −50 °C, the sample appeared as in Figure 4A. The mottled appearance of the high-relief phase labeled ice V is probably due to some ice I sandwiched between ice V and the diamond-anvil faces. In the temperature range −67 to −69 °C, the appearance of the sample changed to that shown in Figure 4B. We suspect from the volume increase that ice V transformed to ice II. On warming, the mottled appearance of the ice II mass in Figure 4B changed somewhat, but, at about −31.1 °C, the volume of high-relief mass increased again (Fig. 4C), perhaps signaling the transformation of ice II to ice III. Finally, at −22.1 °C, the ice phases recrystallized (Fig. 4D), presumably facilitated by the presence of liquid. The ice I melted leaving ice III and liquid. The last of the ice III melted at −19.2 °C, indicating a pressure of 2.68 kbar (Wagner et al., 1994) and a density of 1.13 g/cm³ (Saul and Wagner, 1989).

In summary, visual observation of the habit of the liquidus ice phase is usually sufficient for an accurate identification of the polymorph. The differentiation of ice polymorphs in the region of the ice V–ice VI–liquid triple point may be uncertain, but subsolidus behavior may provide the necessary clues. Once the polymorph is identified and the melting point is determined, calculation of the *P-T* path of the isochore is straightforward.

Acknowledgments

We greatly appreciate the reviews of this manuscript by Harvey E. Belkin, Robert J. Bodnar, Gordon L. Nord, Jr., and Jeffrey S. Sweeny.

References cited

Bassett, W.A., Shen, A.H., Bucknum, M., and Chou, I-M. (1993) A new diamond anvil cell for hydrothermal studies to 2.5 GPa and from −190 to 1200°C. Reviews of Scientific Instruments, 64, 2340–2345.

Bridgman, P.W. (1912) Water, in the liquid and five solid forms under pressure. Proceedings of the American Academy of Arts and Sciences, 47, 441–558.

Brodholt, J.P., and Wood, B.J. (1993) Simulations of the structure and thermodynamic properties of water at high pressures and temperatures. Journal of Geophysical Research, 98, 519–536.

——— (1994) Measurements of the *PVT* properties of water to 25 kbars and 1600°C from fluid inclusions in corundum. Geochimica et Cosmochimica Acta, 58, 2143–2148.

Burnham, C.W., Holloway, J.R., and Davis, N.F. (1969) Thermodynamic properties of water to 1,000°C and 10,000 bars. Geological Society of America Special Paper, 132, 96 p.

Chou, I-M., Haselton, H.T., Jr., Nord, G.L., Jr., Shen, A.H., and Bassett, W.A. (1993) Barium titanate as a pressure calibrant in the diamond anvil cells. Eos, 74, 170.

Duan, Z., Møller, N., and Weare, J.H. (1992) An equation of state for the CH_4-CO_2-H_2O system: I. Pure systems from 0 to 1000°C and 0 to 8000 bar. Geochimica et Cosmochimica Acta, 56, 2605–2617.

Evans, L.F. (1967) Selective nucleation of the high-pressure ices. Journal of Applied Physics, 38, 4930–4932.

Haar, L., Gallagher, J.S., and Kell, G.S. (1984) NBS/NRC steam tables: Thermodynamic and transport properties and computer programs for vapor and liquid states of water in SI units, 320 p. Hemisphere, Washington, DC.

Halbach, H., and Chatterjee, N.D. (1982) An empirical Redlich-Kwong-type equation of state for water to 1,000°C and 200 kbar. Contributions to Mineralogy and Petrology, 79, 337–345.

Haselton, H.T., Jr., and Chou, I-M. (1994) A control and acquisition system for use with a hydrothermal diamond-anvil cell. U.S. Geological Survey Open-File Report 94-703, 24 p.

Mirwald, P.W., and Massonne, H.-J. (1980) The low-high quartz and quartz-coesite transition to 40 kbar between 600° and 1600°C and some reconnaissance data on the effect of $NaAlO_2$ component on the low quartz-coesite transition. Journal of Geophysical Research, 85, 6983–6990.

Saul, A., and Wagner, W. (1989) A fundamental equation for water covering the range from the melting line to 1273 K at pressures up to 25000 MPa. Journal of Physical and Chemical Reference Data, 18, 1537–1564.

Sharp, Z.D., Essene, E.J., and Hunziker, J.C. (1993) Stable isotope geochemistry and phase equilibria of coesite-bearing whiteschists, Dora Maira Massif, western Alps. Contributions to Mineralogy and Petrology, 114, 1–12.

Shen, A.H., Bassett, W.A., and Chou, I-M. (1993) The α-β quartz transition at high temperatures and pressures in a diamond-anvil cell by laser interferometry. American Mineralogist, 78, 694–698.

Wagner, W., Saul, A., and Pruss, A. (1994) International equations for the pressure along the melting and along the sublimation curve of ordinary water substance. Journal of Physical and Chemical Reference Data, 23, 515–527.

Zhang, R.Y., and Liou, J.G. (1994) Significance of magnesite paragenesis in ultrahigh-pressure metamorphic rocks. American Mineralogist, 79, 397–400.

Manuscript received January 17, 1995
Manuscript accepted July 6, 1995